Surface impedance anisotropy of $YBa_2Cu_3O_{6.95}$ single crystals: Electrodynamic basis of the measurements

Yu. A. Nefyodov, M. R. Trunin, A. A. Zhohov, I. G. Naumenko, and G. A. Emel'chenko
Institute of Solid State Physics RAS, 142432 Chernogolovka, Moscow district, Russia

D. Yu. Vodolazov and I. L. Maksimov
Nizhny Novgorod University, 23 Gagarin Avenue, Nizhny Novgorod 603600, Russia

(Received 5 June 2002; published 4 April 2003)

An electrodynamic technique is developed for determining the components of surface impedance and complex conductivity tensors of HTSC single crystals on the basis of measured quantities of a quality factor and a resonator frequency shift. A simple formula is obtained for a geometrical factor of a crystal in the form of a plate with dimensions $b \gg a > c$ in a microwave magnetic field $\mathbf{H}_\omega \perp ab$. To obtain the *c*-axis complex conductivity from measurements at $\mathbf{H}_\omega \| ab$, we propose a procedure that takes into account of sample size effects. With the aid of the technique involved temperature dependences of all impedance and conductivity tensors components of $YBa_2Cu_3O_{6.95}$ single crystal, grown in $BaZrO_3$ crucible, are determined at a frequency of $f = 9.4$ GHz in its normal and superconducting states. All of them proved to be linear at $T < T_c/2$, and their extrapolation to zero temperature gives the values of residual surface resistance $R_{ab}(0) \approx 40\ \mu\Omega$ and $R_c(0) \approx 0.8\ \mathrm{m}\Omega$ and magnetic-field penetration depth $\lambda_{ab}(0) \approx 150$ nm and $\lambda_c(0) \approx 1.55\ \mu$m.

DOI: 10.1103/PhysRevB.67.144504 PACS number(s): 74.25.Nf, 74.72.Bk

I. INTRODUCTION

Microwave measurements of the temperature dependence of the complex conductivity tensor $\hat{\sigma}(T) = \hat{\sigma}'(T) - i\hat{\sigma}''(T)$ of high-T_c superconductors (HTSC) have advanced considerably our understanding of the mechanisms of quasiparticles transport along crystallographic axes of these anisotropic compounds. The real part $\hat{\sigma}'(T)$ is susceptible to the scattering rate of quasiparticles, as well as their density of states. The imaginary part $\hat{\sigma}''(T)$ is related to the magnetic-field penetration depth $\lambda(T)$. In the local electrodynamics, which can be applied to HTSC,

$$\hat{\sigma}(T) = i\omega\mu_0/\hat{Z}^2(T), \tag{1}$$

where $\hat{Z}(T)$ is the surface impedance tensor of the sample, $\omega = 2\pi f$ and $\mu_0 = 4\pi \times 10^{-7}$ H/m. In HTSC the tensors $\hat{Z}$ and $\hat{\sigma}$ are characterized by two components: $Z_{ab} = R_{ab} + iX_{ab}$ (or $\sigma_{ab} = \sigma'_{ab} - i\sigma''_{ab}$) in weakly anisotropic ab planes CuO_2 and $Z_c = R_c + iX_c$ ($\sigma_c = \sigma'_c - i\sigma''_c$) perpendicular to these planes.

In the temperature range $T \geqslant T_c$, $R_{ab}(T) = X_{ab}(T)$ in the ab plane of the optimum-doped $YBa_2Cu_3O_{6.95}$ (Refs. 1–5) and $Bi_2Sr_2CaCu_2O_{8+\delta}$ (Refs. 5–7) single crystals, and this relation is equivalent to the condition of the normal skin effect. The common features of these crystals are the linear temperature dependence of the surface resistance [$\Delta R_{ab}(T) \propto T$] and of the surface reactance [$\Delta X_{ab}(T) \propto \Delta\lambda_{ab}(T) \propto T$] at temperatures $T \ll T_c$ (see Refs. 8–11 and references therein). The difference is that the linear resistivity region extends to near $T_c/2$ for $Bi_2Sr_2CaCu_2O_{8+\delta}$ and terminates near or below $T < T_c/3$ for $YBa_2Cu_3O_{6.95}$ single crystals. At higher temperatures, $R_s(T)$ of $YBa_2Cu_3O_{6.95}$ has a broad peak. In addition, the $\lambda_{ab}(T)$ curves of some $YBa_2Cu_3O_{6.95}$ single crystals have unusual features in the intermediate temperature range.[4,12]

In comparison with the microwave response of the cuprate layers of HTSC, the data concerning their microwave properties in the direction perpendicular to these layers are scarce. Moreover, the available experimental data are controversial. In this connection, the major electrodynamic problem is the accuracy of the techniques used in determination of $Z_c(T)$ and $\sigma_c(T)$ in HTSC.

The most convenient technique for measurements of the surface impedance of small HTSC samples in the *X*-*W* microwave frequency bands is the so-called "hot-finger" method.[9,13] The underlying idea of the method is that a crystal is set on a sapphire rod at the center of a superconducting cylindrical cavity resonating at the frequency f in the H_{011} mode, i.e., at the antinode of a quasihomogeneous microwave magnetic field. In the experiment the real R and imaginary X parts of the surface impedance are derived from the following relations:

$$R = \Gamma\Delta(1/Q), \quad X = -2\Gamma\,\delta f/f. \tag{2}$$

Here Γ is the sample geometrical factor; $\Delta(1/Q)$ is the difference between the values $1/Q$ of the cavity with the sample inside and the empty one; δf is the frequency shift relative to that which would be measured for a sample with perfect screening and no penetration of microwave fields. In the experiment we measure the difference $\Delta f(T)$ between resonant frequency shifts versus temperature of the loaded and empty cavity, which is equal to $\Delta f(T) = \delta f(T) + f_0$, where f_0 is a constant. In HTSC single crystals the constant f_0 can be determined from measurements of the surface im-

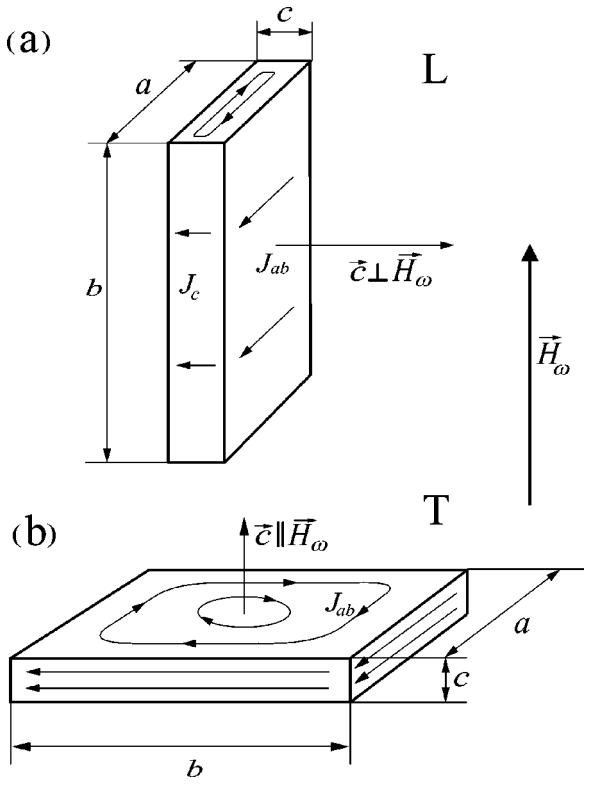

FIG. 1. Two experimental orientations of the sample with respect to the microwave magnetic-field $\mathbf{H}_\omega$, (a) longitudinal L orientation, $\mathbf{H}_\omega \| ab$, and (b) transverse T orientation, $\mathbf{H}_\omega \perp ab$. Arrows indicate the direction of the high-frequency currents.

pedance in the normal state.[14] Another quantity essential for determining the values of $R(T)$ and $X(T)$ from Eq. (2) is the sample geometric factor

$$\Gamma = \frac{2\omega W}{\gamma}, \quad W = \frac{\mu_0}{2}\int_V H_\omega^2 dV, \quad \gamma = \int_s H_t^2 ds, \qquad (3)$$

where W is the energy stored in the cavity, V is the volume of the cavity, $\mathbf{H}_\omega$ is the microwave magnetic field generated in the cavity, s is the total sample surface area, and $\mathbf{H}_t$ is the tangential component of $\mathbf{H}_\omega$ on the sample surface. The energy W is easily obtained for the resonator mode under use, therefore the task of deriving the impedance value is reduced to defining the integral γ in Eq. (3). The task simplifies if a typical HTSC crystal in the form of a rectangular plate with dimensions $b \gg a > c$ and volume $v \sim 0.1$ mm^3 is radiated by the microwave magnetic field $\mathbf{H}_\omega \| b$ [L orientation, Fig. 1(a)]. If this is the case, in the superconducting state at $T < 0.9T_c$, when the magnetic-field penetration depth is smaller than the characteristic sample dimensions, the quantity $H_t \simeq H_0$ can be taken out of the integral γ, where H_0 is an amplitude of $\mathbf{H}_\omega$. Thus we obtain $\gamma \simeq 2H_0^2(ab+bc)$, so the surface impedance Z_{ab+c} for the sample in the L orientation will be equal to

$$Z_{ab+c} \simeq \frac{abZ_{ab}+bcZ_c}{ab+bc}, \qquad (4)$$

where the subscripts of Z denote the directions of the screening currents. While deriving formula (4) we neglect not only weak anisotropy in the ab plane but also a contribution of the crystal ac faces which is apparently minute in comparison with the summands in the numerator in Eq. (4) due to the areas difference $ac \ll bc < ab$. The cleaving of the crystal along the b edge into several needles multiplies up the contribution from the c axis, so that measurements of Z_{ab+c} before and after the cleaving allowed to extract Z_c in the superconducting state of $YBa_2Cu_3O_{6.95}$ single crystal.[15] However, this procedure has the following disadvantages: (i) it assumes abZ_{ab} term in Eq. (4) to be nonalterable, which results in an uncontrolled inaccuracy due to nonideal sample cleaving into rectangular needles, (ii) as it will be shown below, the size effect takes place at temperatures $T > 0.9T_c$ in the L orientation; this restricts applicability range of Eq. (4) within low temperatures and does not allow to extract $\lambda_c(0)$ value, and (iii) in many cases one needs to save the initial sample for further study, e.g., for investigation of evolution of its anisotropic properties with doping level.

Therefore, consecutive measurements of the crystal at first in transverse (T) orientation $\mathbf{H}_\omega \| c$ [Fig. 1(b)] to obtain Z_{ab} and then in longitudinal (L) one appear to be a more natural way to obtain Z_c value. A difficulty in determining the geometrical factor Γ or the integral γ in Eq. (3) in the T orientation of the crystal arises while using this technique. As mentioned in Ref. 9, $\gamma \simeq 2H_0^2a^2[\ln(a/c)+1]$ proves to be a reasonable estimation for a square sample with $a=b \gg c$. It is also known that the approximation of a rectangular plate to an ellipsoid inscribed in it results in an overestimated value of γ.

The purpose of this paper is (i) to calculate γ for a typical HTSC crystal in the T orientation, (ii) to generalize formula (4) for the L orientation of the crystal to the range of higher temperatures $T > 0.9T_c$, and (iii) to report on the measurement results for all surface impedance components of high-quality $YBa_2Cu_3O_{6.95}$ single crystals, grown in $BaZrO_3$ crucibles, in the normal and superconducting states.

II. GEOMETRICAL FACTOR IN THE *T* ORIENTATION

Let us consider a rectangular ideal conductor with dimensions $L_y \gg L_x, L_z$ placed in a constant magnetic field $\mathbf{H} \| z$ (Fig. 2). The problem of obtaining the field distribution around such a conductor becomes two dimensional and to solve it one can apply the method suggested in Ref. 16. The magnetic field outside the conductor satisfies Maxwell equations $\nabla \times \mathbf{H} = 0$ and $\nabla \cdot \mathbf{B} = 0$. The former equation allows to introduce a scalar potential φ, and the latter allows to introduce a vector potential $\mathbf{A}$: $\mathbf{H} = -\nabla \cdot \varphi = \nabla \times \mathbf{A}/\mu_0$. Let $\mathbf{A}$ be directed along the y axis: $\mathbf{A} = (0,A,0)$. Then the magnetic-field components will be as follows:[17]

$$H_x - iH_z = -\frac{d\psi}{dw}, \qquad (5)$$

where the complex potential $\psi = \varphi + iA/\mu_0$ is an analytical function of $w = x + iz$ variable, which determines the conformal mapping of (x,z) plane into $(\varphi, A/\mu_0)$ plane. Schwarz transformation

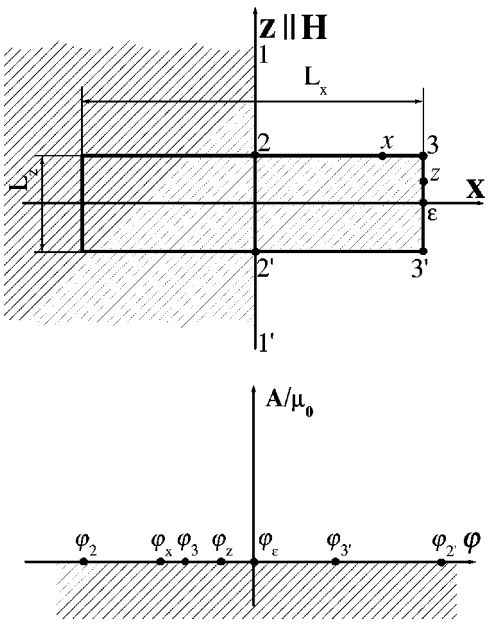

FIG. 2. Complex planes (x,z) and $(\varphi,A/\mu_0)$ used for conformal mapping.

$$\frac{dw}{d\psi}=-\frac{i}{H}\sqrt{\frac{(\psi-\psi_3)(\psi-\psi_{3'})}{(\psi-\psi_2)(\psi-\psi_{2'})}} \tag{6}$$

specifies the relationship between the unshaded areas in Fig. 2. Placing the point ψ_ϵ into plain $(\varphi,A/\mu_0)$ point of origin, we get $\varphi_\epsilon=0$ and $A=0$ $(\psi=\varphi)$ along the path $1\to2\to3\to\epsilon\to3'\to2'\to1'$. Owing to the task symmetry $\varphi_2=-\varphi_{2'}$ and $\varphi_3=-\varphi_{3'}$. Integrating Eq. (6), we obtain the following relationship between x,z coordinates and potential φ on the conductor surface:

$$x=-\frac{\varphi_3}{H}\frac{\sqrt{1-k^2}}{k}E\left(\sqrt{1-\frac{\varphi^2}{\varphi_2^2}},\frac{1}{\sqrt{1-k^2}}\right)$$

$$(z=L_z/2,\ \ 0\leqslant x\leqslant L_x/2),$$

$$z=-\frac{\varphi_3}{H}E\left(\frac{\varphi}{\varphi_2},\frac{1}{k}\right)\quad (x=L_x/2,0\leqslant z\leqslant L_z/2), \tag{7}$$

where $k=\varphi_3/\varphi_2$, and $E(u,v)$ is an incomplete elliptic integral of the second kind. Equations (5) and (7) define an implicit dependence of the magnetic field against coordinates on the conductor surface. The upper inset in Fig. 3 displays the distribution of $H_z(z)$ and $H_x(x)$ magnetic-field components in L_zL_y and L_xL_y planes, respectively, for three different L_z/L_x ratios.

From the formulas (5)–(7) one can easily calculate the magnetic moment of the conductor

$$M=\left|\frac{1}{2}\int \mathbf{j}\times\mathbf{r}\,dv\right|=-4L_y\left(\int_0^{L_x/2}x|H_x|dx+\frac{L_x}{2}\int_0^{L_z/2}H_z dz\right) \tag{8}$$

and the integral γ in Eq. (3),

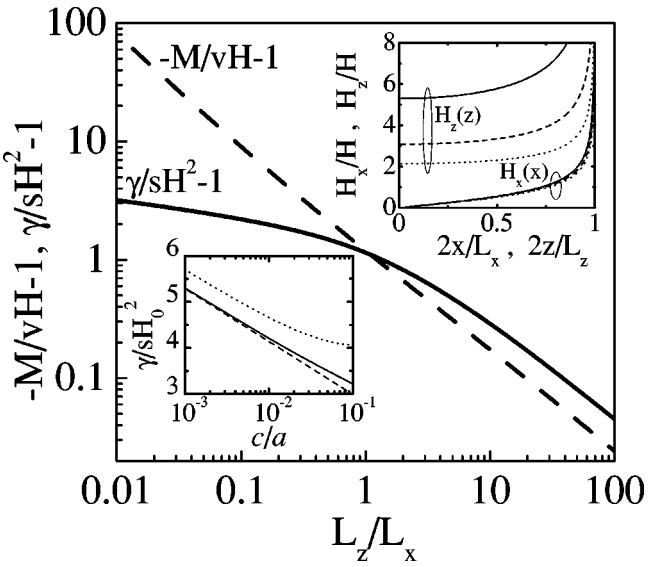

FIG. 3. The values of $[-M/vH-1]$ (dashed line) and $[\gamma/sH^2-1]$ (solid line) calculated from Eqs. (10) and (11) versus the ratio L_z/L_x. The upper inset represents the magnetic-field distribution on the surfaces L_zL_y (upper three curves) and L_xL_y (lower curves) for the values of $L_z/L_x=0.25$ (dotted lines), 0.1 (dashed lines), and 0.03 (solid lines). The lower inset, γ/sH_0^2 as a function of c/a. Solid and dashed lines correspond to the calculations of Eqs. (11) and (14), respectively. Dotted line is the upper limit of γ/sH_0^2 estimated from Eq. (15) for $b=4a$.

$$\gamma=4L_y\left(\int_0^{L_x/2}H_x^2dx+\int_0^{L_z/2}H_z^2dz\right). \tag{9}$$

In order to obtain this we change from integration over coordinates in Eqs. (8) and (9) to integration over potential, taking formulas (5) and (6) into account,

$$-\frac{M}{L_yH}=\frac{4}{H}\left(\int_{\varphi_2}^{\varphi_3}xd\varphi-\frac{L_x}{2}\int_0^{\varphi_3}d\varphi\right)$$

$$=\frac{\pi(1-k^2)L_z^2}{4}[E(k)-(1-k^2)K(k)]^2, \tag{10}$$

$$\frac{\gamma}{L_yH^2}=\frac{4}{H}\left(\int_{\varphi_2}^{\varphi_3}\sqrt{\frac{\varphi_2^2-\varphi^2}{\varphi^2-\varphi_3^2}}d\varphi+\int_{\varphi_3}^{0}\sqrt{\frac{\varphi_2^2-\varphi^2}{\varphi_3^2-\varphi^2}}d\varphi\right)$$

$$=2(L_xf_x+L_zf_z), \tag{11}$$

where

$$f_x=\frac{K(\sqrt{1-k^2})-E(\sqrt{1-k^2})}{E(\sqrt{1-k^2})-k^2K(\sqrt{1-k^2})},$$

$$f_z=\frac{E(k)}{E(k)-(1-k^2)K(k)}, \tag{12}$$

with $K(v)$ and $E(v)$ being complete elliptic integrals of the first and second kinds. Formula (10) coincides with the result obtained previously in Ref. 18. Furthermore, the relationship

between the ratio L_z/L_x and k is required to calculate the values of the moment M/v ($v=L_xL_yL_z$ is a conductor volume) and the factor γ/s [$s=2L_y(L_z+L_x)$ is a conductor surface area], which we obtain substituting the values $x=L_x/2$ and $z=L_z/2$ into the left side of Eq. (7),

$$\frac{L_z}{L_x}=\frac{E(k)-(1-k^2)K(k)}{E(\sqrt{1-k^2})-k^2K(\sqrt{1-k^2})}. \tag{13}$$

M and γ dependences on L_z/L_x ratio, computed from formulas (10) and (11), are presented in Fig. 3. If $L_z \gg L_x$, the magnitude of the magnetic field on the sample surface tends to that of the applied one along with the values of M and γ tending to $(-vH)$ and sH^2, respectively.

Presently we apply the formulas obtained to determe the HTSC crystal geometrical factor when transversely placed with respect to $\mathbf{H}_\omega$ field [Fig. 1(b)]. The field distribution on the ideal conductor surface will coincide with alternating magnetic-field distribution on the surface of a superconducting sample of the same dimensions ($L_x=a, L_y=b, L_z=c$) placed in microwave field $\mathbf{H}_\omega=\mathbf{H}$, provided that the penetration depth is smaller than the sample dimensions. It is easy to obtain a simple estimation of γ in case of a very thin crystal ($c \ll a \ll b$). Upon keeping the first term from the expansion into $k \ll 1$ series of the right side of Eq. (13), we get the value $k \simeq \sqrt{4L_z/\pi L_x}$. Therefore, small values of k correspond to $c/a \ll 1$. The subsequent substitution of $k=\sqrt{4c/\pi a}$ into asymptotic forms $f_x(k) \simeq K(\sqrt{1-k^2})-1$, $f_z(k) \simeq 2/k^2$ with $k \ll 1$ in Eq. (12) gives the following from Eq. (11):

$$\gamma \simeq 2H_0^2 ab\left(\frac{\pi}{2}-1+\frac{1}{2}\ln\frac{4\pi a}{c}\right). \tag{14}$$

The lower inset in Fig. 3 represents the comparison of γ values obtained from the general formula (11) and the asymptotic one (14).

Let us now consider the influence of a finite crystal length (b dimension) on the γ quantity. Taking an arising additional contribution from ac faces of the crystal [Fig. 1(b)] into account and assuming a tangential field component on these faces to be the same as that on the other lateral bc faces, from Eq. (11) we obtain

$$\gamma=2H_0^2(abf_x+bcf_z+acf_z). \tag{15}$$

However, estimation (15) gives an overestimated value of γ in the case of a real three-dimensional sample. Indeed, the limitation of the crystal length b will result in a decrease of the magnetic-field tangential component $\mathbf{H}_t \| a$ on the sample surface. The appropriate decrease in γ will not be compensated by the appearance of $\mathbf{H}_t \| b$ component, which is absent when $b \to \infty$. Thus, formula (15) is an upper limit of γ, and its c/a dependence is shown in the lower inset of Fig. 3.

In order to check the accuracy of the above calculations we have measured both magnetic moment M and geometrical factor γ of superconducting slabs with different a/c and b/a ratios using ac susceptibility and cavity perturbation techniques. The discrepancy between theoretical and experimentally obtained values of M reached up to 20% in case of short ($b \sim 3a$) samples and decreased to less than 5% for substantially long samples ($b \sim 6a$). In contrast to magnetic moment, the values of γ proved to be in better agreement with the theory. In fact, divergence have never exceeded 5%, probably, due to weaker (logarithmic) dependence of γ on a/c ratio.

Both M and γ integrals in Eqs. (8) and (9) are convergent. At the same time, as follows from Eqs. (5) and (6), the magnetic field diverges $\propto 1/r^{1/3}$ at small distances r from the edges (point 3 in the Fig. 2). In this connection the question arises about possible nonlinearities on the edges of the superconducting slab. In the resonant circuits we applied small amplitude ($H_0 < 0.1$ Oe) of the ac magnetic field. The one-order increase of H_0 did not give rise to any nonlinear effects under the measurements of $YBa_2Cu_3O_{6.95}$ crystals.

III. ELECTRODYNAMICS OF ANISOTROPIC CRYSTAL

The electrodynamics of a layered anisotropic HTSC is characterized by components σ_{ab} and σ_c of the conductivity tensor. In the normal state ac field penetrates along the c axis through a skin depth $\delta_{ab}=\sqrt{2/\omega\mu_0\sigma_{ab}}$ and in the CuO_2 plane through $\delta_c=\sqrt{2/\omega\mu_0\sigma_c}$. In the superconducting state all parameters δ_{ab}, δ_c, $\sigma_{ab}=\sigma'_{ab}-i\sigma''_{ab}$, and $\sigma_c=\sigma'_c-i\sigma''_c$ are complex. At $T<T_c$, if $\sigma' \ll \sigma''$ the field penetration depths are given by formulas $\lambda_{ab}=\sqrt{1/\omega\mu_0\sigma''_{ab}}$, $\lambda_c=\sqrt{1/\omega\mu_0\sigma''_c}$. In the close neighborhood of T_c, decay of the magnetic-field in a superconductor is characterized by functions $\mathrm{Re}(\delta_{ab})$ and $\mathrm{Re}(\delta_c)$, which turn to δ_{ab} and δ_c at $T \geqslant T_c$, respectively.

In the T orientation the surface impedance Z_{ab} is directly connected with the in-plane penetration depth $\lambda_{ab}(T)$ at $T<T_c$ and the skin depth $\delta_{ab}(T)$ at $T \geqslant T_c$. Both lengths are smaller than the typical crystal thickness. Hence, when the crystal is in the T orientation and at an arbitrary temperature the surface impedance Z_{ab} is defined as a coefficient in Leontovich boundary condition,[17] and is correlated with the conductivity σ_{ab} through the local relation

$$Z_{ab}=R_{ab}+iX_{ab}=\left(\frac{i\omega\mu_0}{\sigma_{ab}}\right)^{1/2}. \tag{16}$$

In case the HTSC microwave conductivity is real in the normal state the real and imaginary parts of the surface impedance are equal. Hence, in the T orientation the constant f_0, essential to determine $X_{ab}(T)$ in Eq. (1), may be found as a result of $R_{ab}(T)$ and $\Delta X_{ab}(T)$ coincidence at $T \geqslant T_c$. It should be pointed out that thermal expansion of the crystal may essentially affect the shape of $X_{ab}(T)$ curve in the T orientation. Since the resonance frequency depends on the volume occupied by the field, the crystal expansion is equivalent to a reduction in the magnetic-field penetration depth and results in an additional frequency shift $\Delta f_l(T)$ of the cavity:[9]

$$\Delta f_l(T)=\frac{f\mu_0}{8W}\int_s \Delta l_i(T)H_t^2 ds$$

$$=\frac{f\mu_0 v H_0^2}{4W}[\varepsilon_c f_x+(\varepsilon_a+\varepsilon_b)f_z], \qquad (17)$$

where ε_i is a relative change $\Delta l_i/l_i$ of the sample dimension l_i (a,b,c) resulting from the thermal expansion, and the functions f_x and f_z are defined according to Eq. (12). In Ref. 9 the contribution (17) to the overall frequency shift is shown to be negligible at low temperatures, however, it becomes noticeable at $T>0.9T_c$ in the T orientation.

In the L orientation at $T<0.9T_c$ the penetration depth in an HTSC crystal is still smaller than characteristic sample dimensions. It allows to treat the experimental data in terms of impedance Z_{ab+c} averaged over the sample surface in accordance with Eq. (4). In particular, taking account of the measurements of $\Delta\lambda_{ab}(T)=\Delta X_{ab}(T)/\omega\mu_0$ in the T orientation and the measured value $\Delta\lambda_{ab+c}(T)=\Delta X_{ab+c}(T)/\omega\mu_0$ in the L orientation, we obtain

$$\Delta\lambda_c=[(a+c)\Delta\lambda_{ab+c}-a\Delta\lambda_{ab}]/c. \qquad (18)$$

This technique of $\Delta\lambda_c(T)$ determination was used in microwave experiments[3,6,15,19–23] at low temperatures $T<T_c$. Nevertheless, this approach to investigation of the surface impedance anisotropy in HTSC crystals at $T<T_c$ does not allow to determine the value of $\lambda_c(T)$ from the measurements of quality factor and resonance frequency shift, nor may it be extended to the range of higher temperatures. The point is that the size effect provides with an essential influence in the L orientation at $T>0.9T_c$, when the penetration depths λ_c and δ_c turn out to be comparable with the crystal width. As a result, the $R_{ab+c}(T)$ temperature dependence measured in the normal state does not coincide with $X_{ab+c}(T)$, which makes the previous method of determining f_0 nonapplicable.

In this case in order to analyze our measurements in both the superconducting and normal states we shall use the formulas for field distribution in an anisotropic long strip ($b\gg a,c$) in the L-orientation.[24] These formulas neglect the effect of the bc faces of the crystal [Fig. 1(a)], but allow for the size effect correctly. At an arbitrary temperature the measured quantities $\Delta(1/Q)$ and $\Delta f(T)=\delta f(T)+f_0$ are expressed in terms of a complex function $\mu(T)=\mu'(T)-i\mu''(T)$:[7,25]

$$\Delta\left(\frac{1}{Q}\right)-2i\frac{\delta f}{f}=\frac{i\mu_0\mu v H_0^2}{2W}, \qquad (19)$$

which is controlled by the components $\sigma_{ab}(T)$ and $\sigma_c(T)$ of the conductivity tensor through the complex penetration depths δ_{ab} and δ_c:

$$\mu=\frac{8}{\pi^2}\sum_n \frac{1}{n^2}\left\{\frac{\tan(\alpha_n)}{\alpha_n}+\frac{\tan(\beta_n)}{\beta_n}\right\},$$

$$\alpha_n^2=-\frac{a^2}{\delta_c^2}\left(\frac{i}{2}+\frac{\pi^2}{4}\frac{\delta_{ab}^2}{c^2}n^2\right),$$

$$\beta_n^2=-\frac{c^2}{\delta_{ab}^2}\left(\frac{i}{2}+\frac{\pi^2}{4}\frac{\delta_c^2}{a^2}n^2\right), \qquad (20)$$

where the sum is performed over odd integers $n>0$.

If $\sigma'\ll\sigma''$ in the superconducting state, we get

$$\mu'\simeq\frac{8}{\pi^2}\sum_n \frac{1}{n^2}\left\{\frac{\tanh(\tilde{\alpha}_n)}{\tilde{\alpha}_n}+\frac{\tanh(\tilde{\beta}_n)}{\tilde{\beta}_n}\right\},$$

$$\tilde{\alpha}_n^2=\frac{a^2}{\lambda_c^2}\left(\frac{1}{4}+\frac{\pi^2}{4}\frac{\lambda_{ab}^2}{c^2}n^2\right),$$

$$\tilde{\beta}_n^2=\frac{c^2}{\lambda_{ab}^2}\left(\frac{1}{4}+\frac{\pi^2}{4}\frac{\lambda_c^2}{a^2}n^2\right). \qquad (21)$$

In particular, $\lambda_{ab}\ll c$ and $\lambda_c\ll a$ at $T<0.9T_c$, so we derive from Eq. (21) a simple expression for the real part of μ:

$$\mu'=2\lambda_c/a+2\lambda_{ab}/c. \qquad (22)$$

One can easily check up that in the range of low temperatures the change in $\Delta\lambda_c(T)$ prescribed by Eq. (22) is identical to that in Eq. (18).

In the normal state the conductivity $\sigma'\gg\sigma''$. If the sample dimensions were much more than the penetration depths, we would obtain the following from Eqs. (19) and (20):

$$\Delta\left(\frac{1}{Q}\right)-2i\frac{\delta f}{f}\simeq(1+i)\frac{\mu_0 v H_0^2}{2W}\left(\frac{\delta_c}{a}+\frac{\delta_{ab}}{c}\right), \qquad (23)$$

i.e., the temperature dependences of $\Delta(1/Q)$ and $(-2\delta f/f)$ would be identical at $T>T_c$, and the values $R_{ab+c}(T)$ and $X_{ab+c}(T)$, derived from Eqs. (2)–(4), would be equal. In practice, the value $\delta_c\sim 0.1$ mm ($f\sim 10$ GHz) proves to be comparable with the crystal width a even for $YBa_2Cu_3O_{6.95}$ crystals, which can be referred to as weakly anisotropic in comparison with other layered HTSC's. So to determine the surface impedance components from the measurements in the L orientation it is necessary to use general formulas (19) and (20), as shown below.

IV. EXPERIMENTAL RESULTS

$YBa_2Cu_3O_{6.95}$ single crystals were grown using the method of slow cooling from a solution-melt with the use of a $BaZrO_3$ crucible. The initial mixture was prepared from a mixture of oxides with mass portions Y_2O_3:BaO_2:CuO =1:25:24 and subsequent pressing of the compound into a tablet of 40 mm in diameter under the pressure of 200 MPa. The initial components purities were 99.95% for both yttrium and copper oxides and 99.90% for barium peroxide. Crucible material porosity (2%) was taken into account when choosing a heating regime and homogenization time. Preliminary experiments have demonstrated that the melt under use saturates the crucible walls through the whole width (3 mm) during the period of 5–7 h at the working temperature. In 10 h crystals growth terminates due to a complete vanishing of the melt from the crucible. To reduce the melt homog-

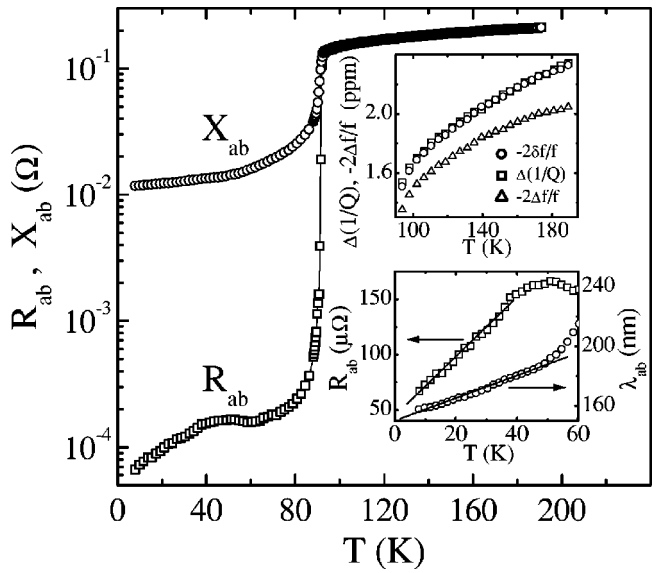

FIG. 4. $R_{ab}(T)$ and $X_{ab}(T)$ of $YBa_2Cu_3O_{6.95}$ single crystal (T orientation). The upper inset shows the measured temperature dependences $-2\Delta f/f$ (triangles) and $\Delta(1/Q)$ (squares). Taking the constant f_0 and thermal expansion into account we get $-2\delta f/f$ (circles). The lower inset displays $R_{ab}(T)$ and $\lambda_{ab}(T)$ dependences at low T.

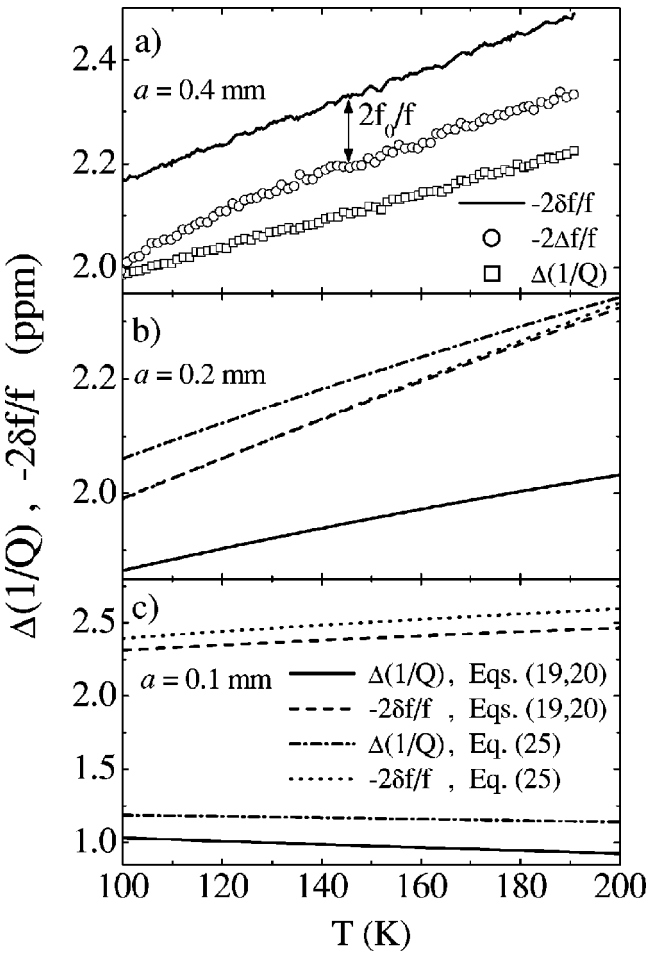

FIG. 5. (a) ΔQ^{-1} (squares) and $-2\Delta f/f$ (circles) measured in the L orientation of $YBa_2Cu_3O_{6.95}$ single crystal at $T \geqslant 100$ K. Solid line shows the temperature dependence of $-2\delta f/f$ derived from Eqs. (19) and (20). The constant $2f_0/f$ is indicated by arrow. (b) ΔQ^{-1} and $-2\delta f/f$ calculated from Eqs. (19) and (20) (solid and dashed lines, respectively) and from Eq. (25) (dash-dotted and dotted lines) for a sample width $a=0.2$ mm. (c) The same as (b) but for $a=0.1$ mm.

enization time which amounts to 10–20 h at 1030 °C, according to Ref. 26, the method of accelerated-decelerated rotation of the crucible[27] was used, which made intensive mixing of the melt possible. The homogenization time of the melt at 1010 °C did not exceed 1 h. Crystals growth time amounted to 2 h at a cooling rate of 3–4 °C/h, after which the remaining melt was decanted at 950 °C and cooled down to room temperature at a rate of 15–20 °C/h. The crystals obtained were saturated with oxygen at 500 °C in an oxygen flow, after which their critical temperature was equal to 92 K. The measurements of the dynamic susceptibility showed that the width of the superconducting transition in the samples did not exceed 0.1 K at 100 KHz.

The surface impedance was measured using the hot-finger technique[9] at a frequency of $f=9.42$ GHz in the T and L orientations.

Figure 4 displays the typical temperature dependences of $R_{ab}(T)$ and $X_{ab}(T)$ for $YBa_2Cu_3O_{6.95}$ single crystal in the normal and superconducting states measured in the T orientation. The sample represented a prolate parallelepiped with dimensions $a\times b\times c=0.4\times 1.6\times 0.1$ mm^3. The sample geometrical factor $\Gamma=90$ kΩ was calculated from Eqs. (11) and (3).

The upper inset in Fig. 4 displays the measured temperature dependences of ΔQ^{-1} (squares) and $-2\Delta f/f$ (triangles) in the normal state of the crystal. The curves $\Delta Q^{-1}(T)$ and $-2\delta f(T)/f=-2[\Delta f(T)+\Delta f_l(T)+f_0]/f$ (circles) coincide after taking into account the additional frequency shift $\Delta f_l(T)$ from Eq. (17), which arises due to the sample thermal expansion,[9,28], along with the constant f_0, which is independent of temperature. The coincidence of $\Delta Q^{-1}(T)$ and $-2\delta f(T)/f$ curves and equality $R_{ab}(T)=X_{ab}(T)$ at $T>T_c$ [according to Eq. (2)] demonstrate the fulfilling of the normal skin effect condition in the ab planes of $YBa_2Cu_3O_{6.95}$ crystal in the T orientation. A linear temperature dependence of resistivity $\rho_{ab}(T)=1/\sigma_{ab}(T)=0.63T$ $\mu\Omega$ cm in the range $100\leqslant T<200$ K together with the skin depth $\delta_{ab}(150\text{ K})=5$ μm are derived from Eq. (16).

The temperature dependence $R_{ab}(T)$ has a broad peak in the range $T\sim T_c/2$, characteristic of $YBa_2Cu_3O_{6.95}$ crystals in the superconducting state. The dependences $R_{ab}(T)$ and $\lambda_{ab}(T)=X_{ab}(T)/\omega\mu_0$ are linear at $T<T_c/3$ (lower inset in Fig. 4). Their extrapolation to $T=0$ K results in the values of residual surface resistance $R_{ab}(0)\approx 40$ $\mu\Omega$ and penetration depth $\lambda_{ab}(0)\approx 150$ nm.

Equations (19) and (20) are used to analyze the experimental data in the L orientation of the crystal. In the normal state the real part of Eq. (19) defines the relationship between $\Delta Q^{-1}(T)$ and the skin depths $\delta_{ab}(T)$ and $\delta_c(T)$. Upon measuring the dependence $\Delta Q^{-1}(T)$ [squares in Fig. 5(a)] at $T>T_c$ in the L orientation and taking the dependence $\delta_{ab}(T)$

$=\sqrt{2\rho_{ab}(T)/\omega\mu_0}$ measured in the T orientation into account, from Eq. (20) we obtain the function $\delta_c(T)=\sqrt{2\rho_c(T)/\omega\mu_0}$, $\delta_c(150\ \mathrm{K})=0.06$ mm, and the temperature dependence $\rho_c(T)=10^4+24T\ \mu\Omega\,\mathrm{cm}$ in the range $100\leqslant T<200$ K. Using already determined dependences $\delta_c(T)$ and $\delta_{ab}(T)$ and having computed the real part $\mu'(T)$ in Eq. (20), from Eq. (19) we calculate $(-2\delta f/f)$ versus temperature at $T>T_c$, which is shown by solid line in Fig. 5(a). This line is approximately parallel to the experimental curve $-2\Delta f(T)/f$ in the L orientation [triangles in Fig. 5(a)] at $T>110$ K. The difference $-2(\delta f-\Delta f)/f$ yields the additive constant f_0. Given f_0 and $\Delta f(T)$ we obtain $\delta f(T)$ in the entire temperature range in the L orientation.

It should be emphasized that the discrepancy of the curves $\Delta Q^{-1}(T)$ and $-2\delta f(T)/f$ at $T>T_c$ in the L orientation does not originate from the thermal expansion of the crystal essential in the T orientation, but arises due to the size effect. This discrepancy becomes more noticeable with the decrease in the crystal width a, when it becomes equal to the skin depth δ_c. The computational result for $\Delta Q^{-1}(T)$ (solid line) and $-2\delta f(T)/f$ (dashed line) from Eqs. (19) and (20) for the above-mentioned dependences $\rho_{ab}(T)$ and $\rho_c(T)$ is shown in Fig. 5(b) and 5(c) for $a=0.2$ mm and $a=0.1$ mm.

It should be noticed that the surface impedance components R_{ab+c} and X_{ab+c} in Eq. (4) cannot be found from the values of $\Delta(1/Q)$ and $\delta f/f$ measured at $T>0.9T_c$ in the L orientation with the use of Eq. (2) due to the size effect in anisotropic HTSC crystals. Moreover, it is also incorrect to substitute the values R and X in these formulas by their effective values $R^{eff}(d)$ and $X^{eff}(d)$ for a thin metal plate of width $d\sim\delta$, placed in microwave field $\mathbf{H}_\omega$ parallel to its infinite surfaces

$$R^{eff}(d)=R\frac{\sinh\eta-\sin\eta}{\cosh\eta+\cos\eta},$$

$$X^{eff}(d)=R\frac{\sinh\eta+\sin\eta}{\cosh\eta+\cos\eta}, \qquad (24)$$

where $\eta=\omega\mu_0 d/2R$, $R=\sqrt{\omega\mu_0\rho/2}$. The point is that though allowing the usage of formulas (24) in Eqs. (2) and (4), the solution of Maxwell equations results in an incorrect (one-dimensional) distribution of high-frequency currents in the crystal. Indeed, for $b\|\mathbf{H}_\omega$ we obtain from Eqs. (2)–(4),

$$\Delta\left(\frac{1}{Q}\right)-2i\frac{\delta f}{f}=\frac{H_0^2}{\omega W}[abZ_{ab}^{eff}(c)+bcZ_c^{eff}(a)], \qquad (25)$$

where the effective values $Z_{ab}^{eff}(c)=R_{ab}^{eff}(c)+iX_{ab}^{eff}(c)$ and $Z_c^{eff}(a)=R_c^{eff}(a)+iX_c^{eff}(a)$ are defined by Eq. (24). Figures 5(b) and 5(c) display the computational result for $\Delta Q^{-1}(T)$ and $-2\delta f(T)/f$ from Eqs. (24) and (25), and above determined dependences $\rho_{ab}(T)$ and $\rho_c(T)$ in the case of two plates of dimensions $a\times b\times c=0.2\times1.6\times0.1$ mm^3 and half the width $a=0.1$ mm. Presently, having compared these results with these obtained from Eqs. (19) and (20), we can see that at $a\approx3\delta_c$ [Fig. 5(b)] approximation (25) proves to be practically insensitive to the size effect, giving rise to weakly differing dependences $\Delta Q^{-1}(T)$ and $-2\delta f(T)/f$ at $T>100$ K. Only in the case of the crystal width $a=0.1$ mm [$a\sim\delta_c$, Fig. 5(c)] does approximation (25) give rise to the result resembling that obtained with the aid of formulas (19) and (20).

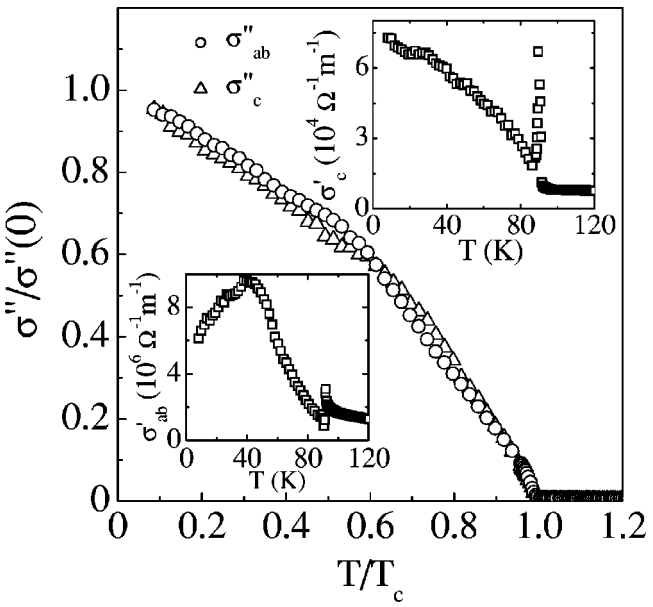

FIG. 6. The conductivities $\sigma''_{ab}/\sigma''_{ab}(0)$ and $\sigma''_c/\sigma''_c(0)$ versus reduced temperature T/T_c. The insets display $\sigma'_{ab}(T)$ and $\sigma'_c(T)$ dependences.

Upon finding the dependences $\Delta Q^{-1}(T)$, $\delta f(T)$ and, hence, the function $\mu(T)$ in Eq. (19) in the normal and superconducting states of $YBa_2Cu_3O_{6.95}$ crystal in the L orientation and using the conductivities $\sigma'_{ab}(T)$ and $\sigma''_{ab}(T)$ found from Eq. (16), we get the c-axis conductivity components $\sigma'_c(T)$ and $\sigma''_c(T)$ from Eq. (20). All the conductivity tensor components obtained are shown in Fig. 6. In case of local relationship between the electric field and the current along the c axis, the surface impedance $Z_c(T)=R_c(T)+iX_c(T)$ is related to the conductivity $\sigma_c(T)=\sigma'_c(T)-i\sigma''_c(T)$ through Eq. (1). Figure 7 displays the components of $Z_c(T)$ obtained in this manner. $R_c(T)$ and $\lambda_c(T)=X_c(T)/\omega\mu_0$ dependences (insets in Fig. 7) demonstrate linear behavior at $T<T_c/2$. The value of the penetration depth along cuprate planes of $YBa_2Cu_3O_{6.95}$ single crystal is equal to $\lambda_c(0)\approx1.55\ \mu$m when extrapolated at zero temperature.

From Eq. (4) one can easily estimate that in the L orientation of our crystal the contribution of the c-axis currents into measurable quantities is about two times greater than that of the ab plane ones: $bcZ_c\approx2abZ_{ab}$. Taking the accuracy of determination of $R_{ab}(T)$ ($<5\%$) and $\Delta\lambda_{ab}(T)$ (a few angstroms) values into account, we conclude that linear behavior of $R_c(T)$ and $\lambda_c(T)$ at low temperatures is the property of optimum-doped $YBa_2Cu_3O_{6.95}$, and is not due to the inaccuracy of the method used. The linear temperature dependence of λ_c at $T<T_c/2$ is also confirmed by the previous microwave[20,23] and low-frequency[29] measurements of $YBa_2Cu_3O_{6.95}$. In contrast to the result of Ref. 15 we did not observe an upturn in $R_c(T)$ at low temperatures. Our surface

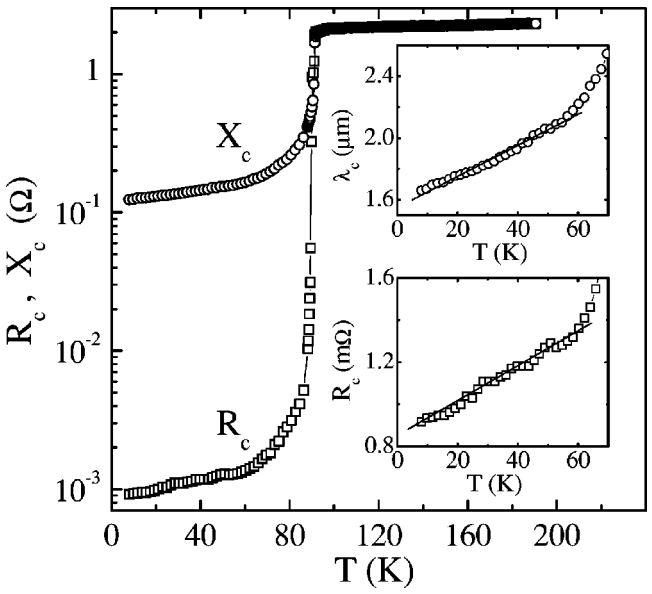

FIG. 7. $R_c(T)$ and $X_c(T)$ of $YBa_2Cu_3O_{6.95}$ single crystal. The insets demonstrate $R_c(T)$ and $\lambda_c(T)$ at low T.

resistance $R_c(T)$ measurements are in qualitative agreement with other microwave data.[3,20]

V. CONCLUSION

In conclusion, we have developed the electrodynamic approach for HTSC surface impedance anisotropy measurements. The major problems in analyzing these measurements in HTSC single crystals are (i) determining the crystal geometrical factor in the T orientation ($\mathbf{H}_\omega \perp ab$), which is dependent on the microwave field distribution on the sample surface; (ii) allowing for the size effect, which influences the quantities measured in the L orientation ($\mathbf{H}_\omega \| ab$) at $T > 0.9T_c$.

We have shown that both these problems may be solved in the case of a crystal in the form of a plate with dimensions $b \gg a > c$. Furthermore, in this case we have calculated the magnetic-field distribution on the crystal surface in the T orientation and found simple expression (11) for its geometric factor. In the L orientation of the crystal, we have shown that only the use of general formulas (19) and (20) allows to take into account of the size effect correctly and to determine the complex conductivity and the surface impedance in the c direction of the crystal in the normal and superconducting states. The experimental technique of measuring all the components of the conductivity tensor is described in detail, and we hope that this technique will be useful in comprehensive studies of anisotropic characteristics of HTSC crystals.

The reported electrodynamic approach has been successfully applied to the analysis of the microwave ($f = 9.4$ GHz) response measurements in both the T and L orientations of $YBa_2Cu_3O_{6.95}$ single crystal, grown in $BaZrO_3$ crucible. The temperature dependences of all conductivity and surface impedance tensors components proved to be linear at $T < T_c/2$. Their extrapolation to zero temperature gives the values of residual surface resistance $R_{ab}(0) \approx 40\ \mu\Omega$ and $R_c(0) \approx 0.8\ \mathrm{m}\Omega$ and magnetic-field penetration depth $\lambda_{ab}(0) \approx 150$ nm and $\lambda_c(0) \approx 1.55\ \mu$m.

ACKNOWLEDGMENTS

We thank P. Monod for helpful discussions. This research has been supported by RFBR Grants Nos. 00-02-17053, 02-02-06578, 02-02-08004 and Government Program on Superconductivity (Contract No. 540-02). M.R.T. thanks Russian Science Support Foundation.

[1] T. Shibauchi, A. Maeda, H. Kitano, T. Honda, and K. Uchinokura, Physica C **203**, 315 (1992).
[2] D. Achkir, M. Poirier, D.A. Bonn, R. Liang, and W.N. Hardy, Phys. Rev. B **48**, 13 184 (1993).
[3] H. Kitano, T. Shibauchi, K. Uchinokura, A. Maeda, H. Asaoka, and H. Takei, Phys. Rev. B **51**, 1401 (1995).
[4] M.R. Trunin, A.A. Zhukov, G.A. Emel'chenko, and I.G. Naumenko, Pis'ma Zh. Eksp. Teor. Fiz. **65**, 893 (1997) [JETP Lett. **65**, 938 (1997)].
[5] T. Shibauchi, H. Kitano, A. Maeda, H. Asaoka, H. Takei, I. Shigaki, T. Kimura, K. Kishio, K. Izumi, T. Suzuki, and K. Uchinokura, J. Phys. Soc. Jpn. **65**, 3266 (1996).
[6] T. Jacobs, S. Sridhar, Q. Li, G.D. Gu, and N. Koshizuka, Phys. Rev. Lett. **75**, 4516 (1995).
[7] D.V. Shovkun, M.R. Trunin, A.A. Zhukov, Yu.A. Nefyodov, H. Enriquez, N. Bontemps, A. Buzdin, M. Daumens, and T. Tamegai, Pis'ma Zh. Eksp. Teor. Fiz. **71**, 132 (2000) [JETP Lett. **71**, 92 (2000)].
[8] D. A. Bonn and W. N. Hardy, in *Physical Properties of High Temperature Superconductors V*, edited by D. M. Ginsberg (World Scientific, Singapore, 1995), pp. 7–97.
[9] M.R. Trunin, Usp. Fiz. Nauk **168**, 931 (1998) [Phys. Usp. **41**, 843 (1998)]; J. Supercond. **11**, 381 (1998).
[10] M.R. Trunin, Yu.A. Nefyodov, and H.J. Fink, Zh. Eksp. Teor. Fiz. **118**, 923 (2000) [JETP **91**, 801 (2000)].
[11] M. R. Trunin and A. A. Golubov, in *Spectroscopy of High-T_c Superconductors*, edited by N. M. Plakida (Taylor & Francis, London, 2002).
[12] H. Srikanth, B.A. Willemsen, T. Jacobs, S. Sridhar, A. Erb, E. Walker, and R. Flükiger, Phys. Rev. B **55**, R14 733 (1997).
[13] S. Sridhar and W.L. Kennedy, Rev. Sci. Instrum. **54**, 531 (1988).
[14] M.R. Trunin, Pis'ma Zh. Eksp. Teor. Fiz. **72**, 845 (2000) [JETP Lett. **72**, 583 (2000)].
[15] A. Hosseini, S. Kamal, D.A. Bonn, R. Liang, and W.N. Hardy, Phys. Rev. Lett. **81**, 1298 (1998).
[16] E. Provost, E. Paumier, and A. Fortini, J. Phys. F: Met. Phys. **4**, 439 (1974).
[17] L. D. Landau and E. M. Lifshitz, *Course of Theoretical Physics*, Electrodynamics of Continuous Media Vol. 8 (Fizmatlit, Moscow, 1982/ Pergamon, New York, 1984).

[18] E.H. Brandt and G.P. Mikitik, Phys. Rev. Lett. **85**, 4164 (2000).
[19] T. Shibauchi, H. Kitano, K. Uchinokura, A. Maeda, T. Kimura, and K. Kishio, Phys. Rev. Lett. **72**, 2263 (1994).
[20] J. Mao, D.H. Wu, J.L. Peng, R.L. Greene, and S.M. Anlage, Phys. Rev. B **51**, 3316 (1995).
[21] D.A. Bonn, S. Kamal, K. Zhang, R. Liang, and W.N. Hardy, J. Phys. Chem. Solids **56**, 1941 (1995).
[22] T. Shibauchi, N. Katase, T. Tamegai, and K. Uchinokura, Physica C **264**, 227 (1996).
[23] H. Srikanth, Z. Zhai, S. Sridhar, and A. Erb, J. Phys. Chem. Solids **59**, 2105 (1998).
[24] C.E. Gough and N.J. Exon, Phys. Rev. B **50**, 488 (1994).
[25] M.R. Trunin, Yu.A. Nefyodov, D.V. Shovkun, A.A. Zhukov, N. Bontemps, H. Enriquez, A. Buzdin, M. Daumens, and T. Tamegai, J. Supercond. **14**, 187 (2001).
[26] A. Erb, E. Walker, and R. Flükiger, Physica C **258**, 9 (1996).
[27] E.O. Shulz-Dubois, J. Cryst. Growth **12**, 81 (1971).
[28] C. Meingast, O. Krauf, T. Wolf, H. Wühl, A. Erb, and G. Müller-Vogt, Phys. Rev. Lett. **67**, 1634 (1991).
[29] C. Panagopoulos, J.R. Cooper, T. Xiang, G.B. Peacock, I. Gameson, and P.P. Edwards, Phys. Rev. Lett. **79**, 2320 (1997).